Electronic Supplementally Information (ESI)

for

Bifunctional electrochemical properties on $La_{0.8}Sr_{0.2}Co_{0.8}M_{0.2}O_{3-\delta}$ (M= Ni, Fe, Mn, Cu): efficient elemental doping based on structural and pH-dependent study

J. Cheng,*[a,b] P. Ganesan,*[a] Z. Wang,[b] M. Zhang,[c] G. Zhang,[d] N. Maeda,[a] J. Matsuda,[e] M. Yamauchi,[a] B. Chi[b] and N. Nakashima*[a]

[a]International Institute for Carbon-Neutral Energy Research (I²CNER), Kyushu University, 744 Moto-oka, Nishi-ku, Fukuoka, 819-0395, Japan

[b]Center for Fuel Cell Innovation, State Key Laboratory of Material Processing and Die & Mould Technology, School of Materials Science and Engineering, Huazhong University of Science & Technology, Wuhan, 430074, China

[c]CAS Key Laboratory of Design and Assembly of Functional Nanostructures, and Fujian Provincial Key Laboratory of Nanomaterials, Fujian Institute of Research on the Structure of Matter, Chinese Academy of Sciences, Fuzhou 350002, China

[d]Department of Applied Chemistry, Graduate School of Engineering, The University of Tokyo, 7-3-1 Hongo, Bunkyo-ku, Tokyo 113-8656, Japan

[e]International Research Center for Hydrogen Energy, Kyushu University, 744 Motooka, Nishi-ku, Fukuoka, 819-0395, Japan

*e-mail: chengjunfang979@aoni.waseda.jp; pandian.ganesan.631@m.kyushu-u.ac.jp; nakashima.naotoshi.614@m.kyushu-u.ac.jp
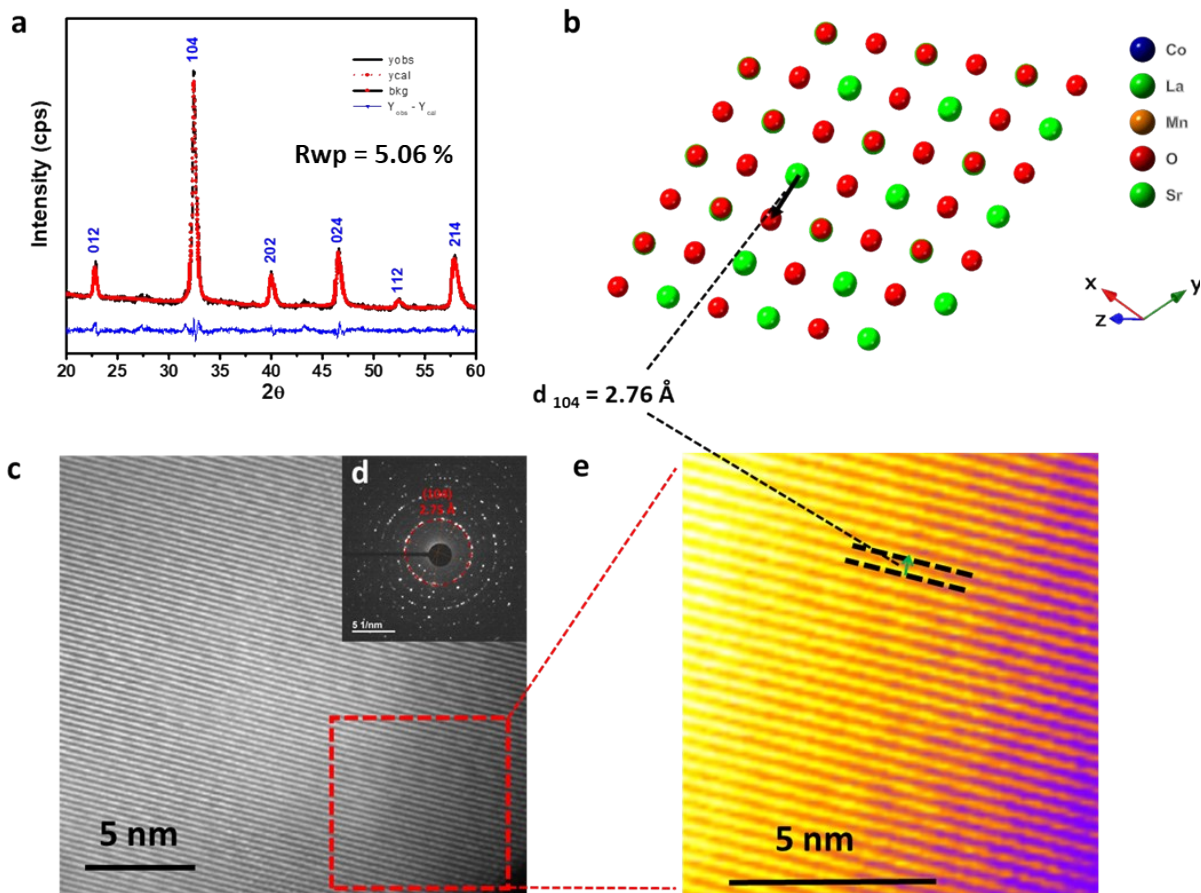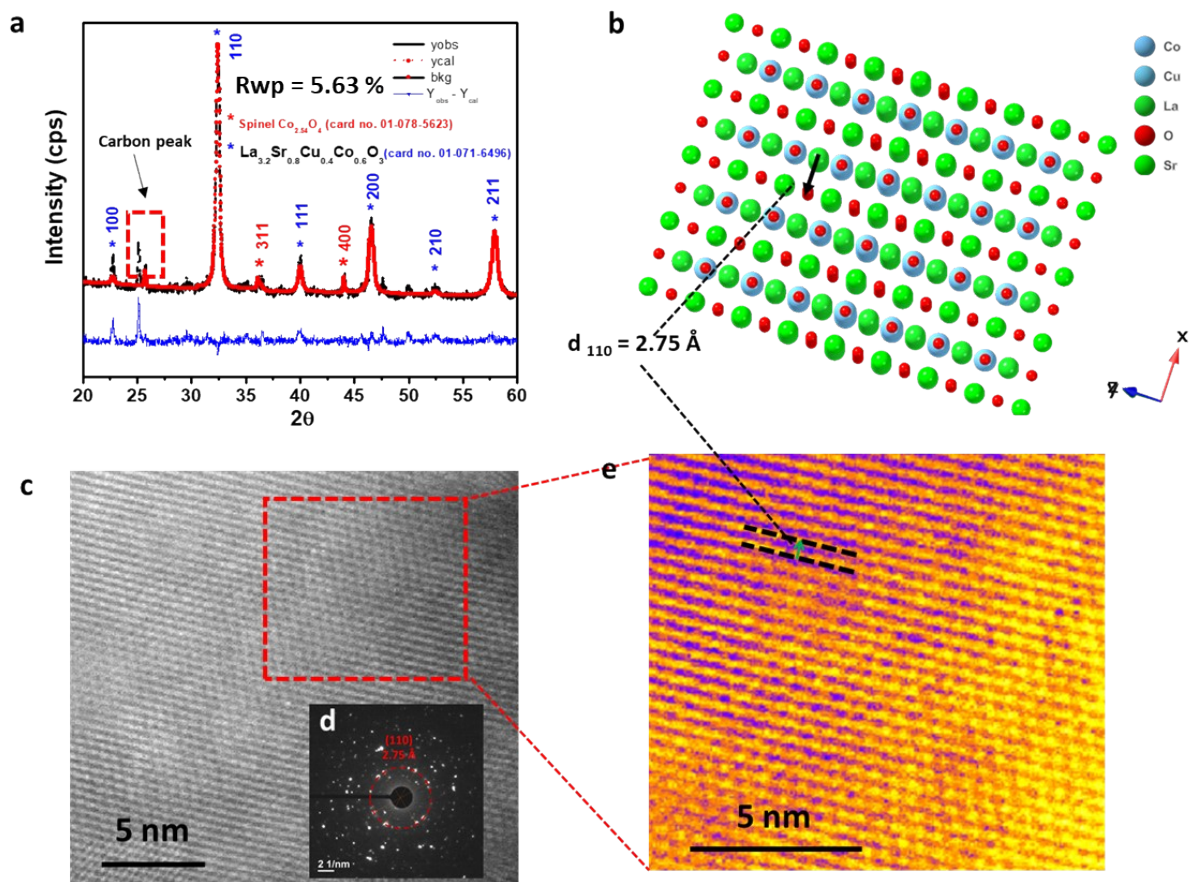
Supporting Figures
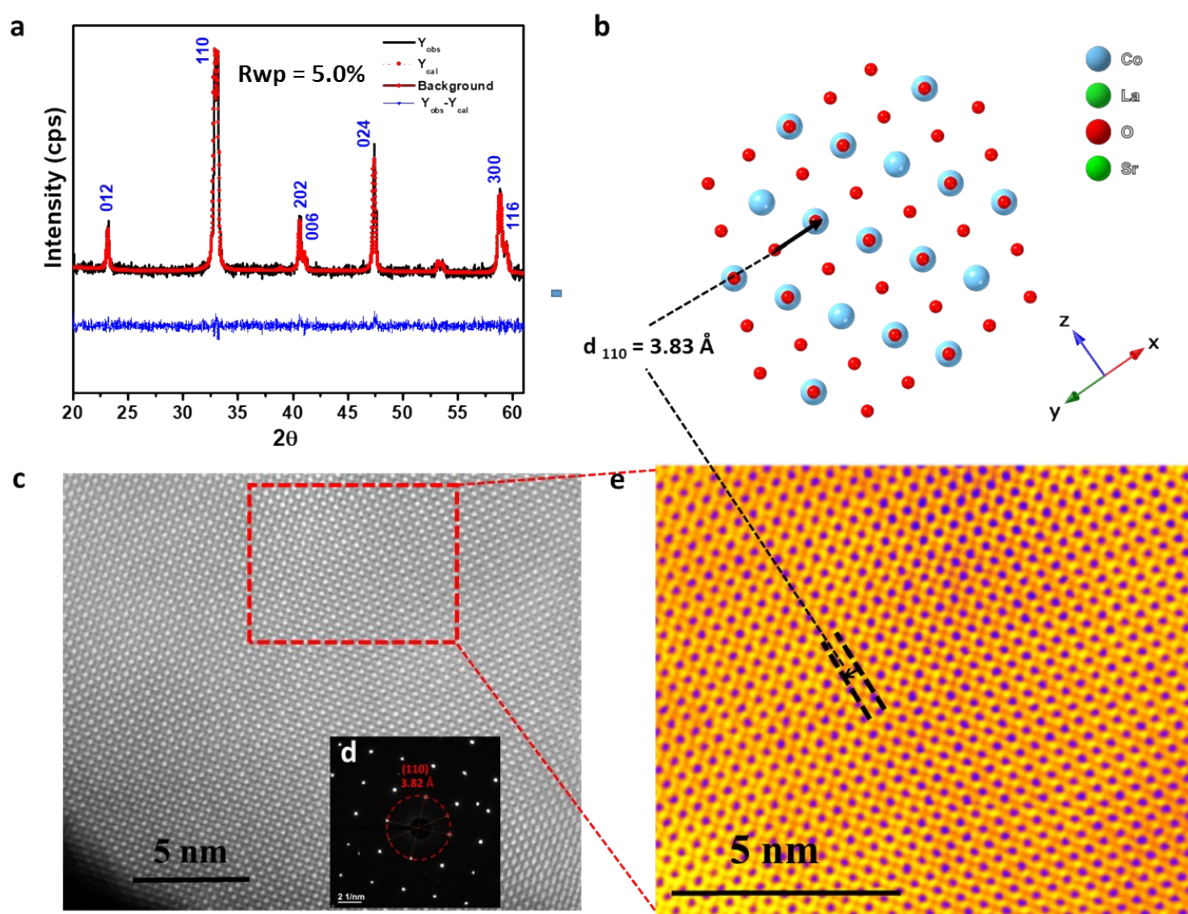
Fig. S1. (a) XRD Rietveld Refinement results, (b) crystal structure, (c) High-angle annular dark-field imaging (HAADF) image and (d) diffraction patterns of $La_{0.8}Sr_{0.2}CoO_{3-\delta}$; (e) the color contrasted images in the red dotted cube area shown in (c). Note: The d-spacing (d_{110}) of crystal structure in (b) and diffraction patterns in (d) are inter-related.
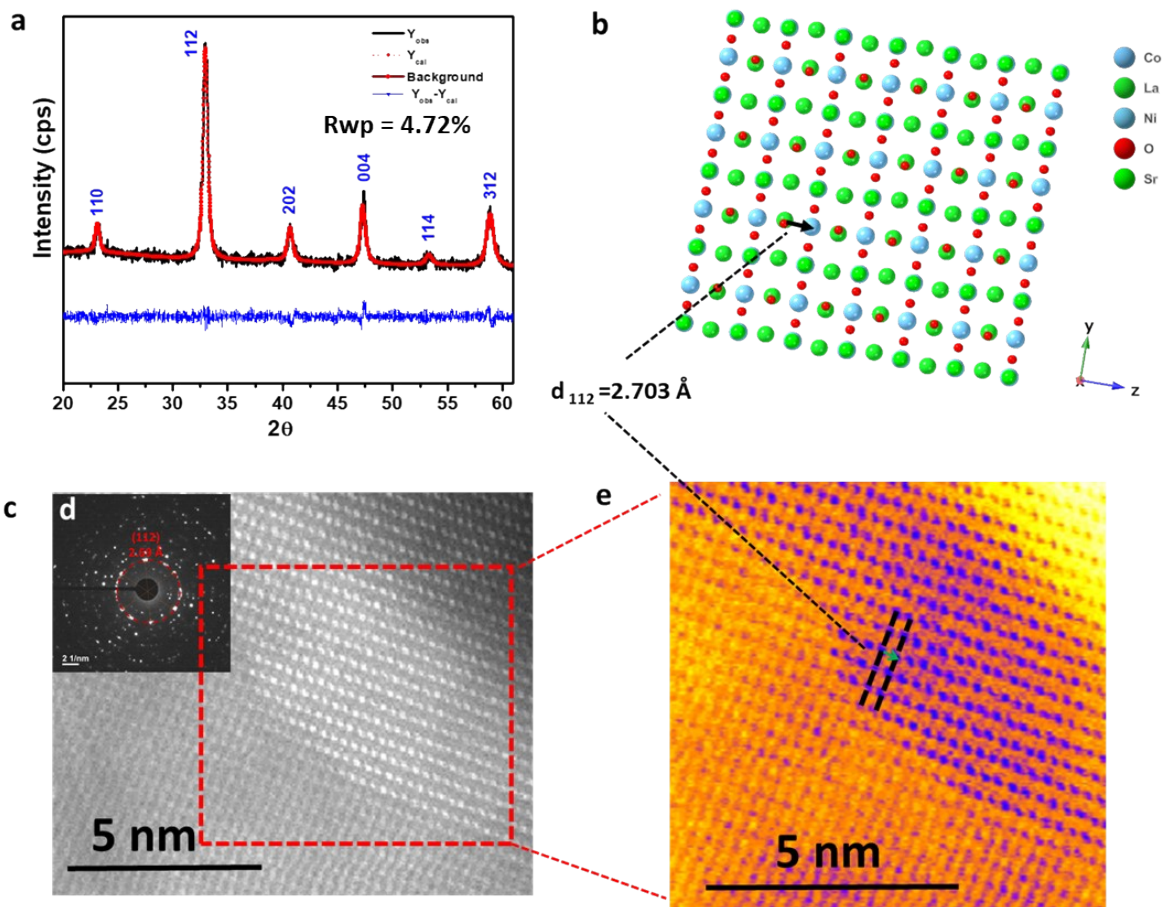
Fig. S2. (a) XRD Rietveld Refinement results, (b) crystal structure obtained from refinement results, (c) High-angle annular dark-field (HAADF) image and (d) diffraction patterns of $La_{0.8}Sr_{0.2}Co_{0.8}Ni_{0.2}O_{3-\delta}$; (e) the color contrasted image of the HAADF pattern in the red dotted cube area shown in (b). Note: The d-spacing (d_{112}) of the (b) and (d) are inter-related.

Fig. S3. (a) XRD Rietveld Refinement results, (b) crystal structure obtained from refinement results, (c) High-angle annular dark-field imaging (HAADF) image and (d) diffraction patterns of $La_{0.8}Sr_{0.2}Co_{0.8}Mn_{0.2}O_{3-\delta}$; (e) the color contrasted image of the HAADF pattern in the red dotted cube area shown in (b). Note: The d-spacing (d_{104}) of the (b) and (d) are inter-related.

Fig. S4. (a) XRD Rietveld Refinement results, (b) crystal structure obtained from refinement results, (c) High-angle annular dark-field imaging (HAADF) image and (d) diffraction patterns of $La_{0.8}Sr_{0.2}Co_{0.8}Cu_{0.2}O_{3-\delta}$; (e) the color contrasted image of the HAADF pattern in the red dotted cube area shown in (b). Note: The d-spacing (d_{104}) of the (b) and (d) are inter-related.
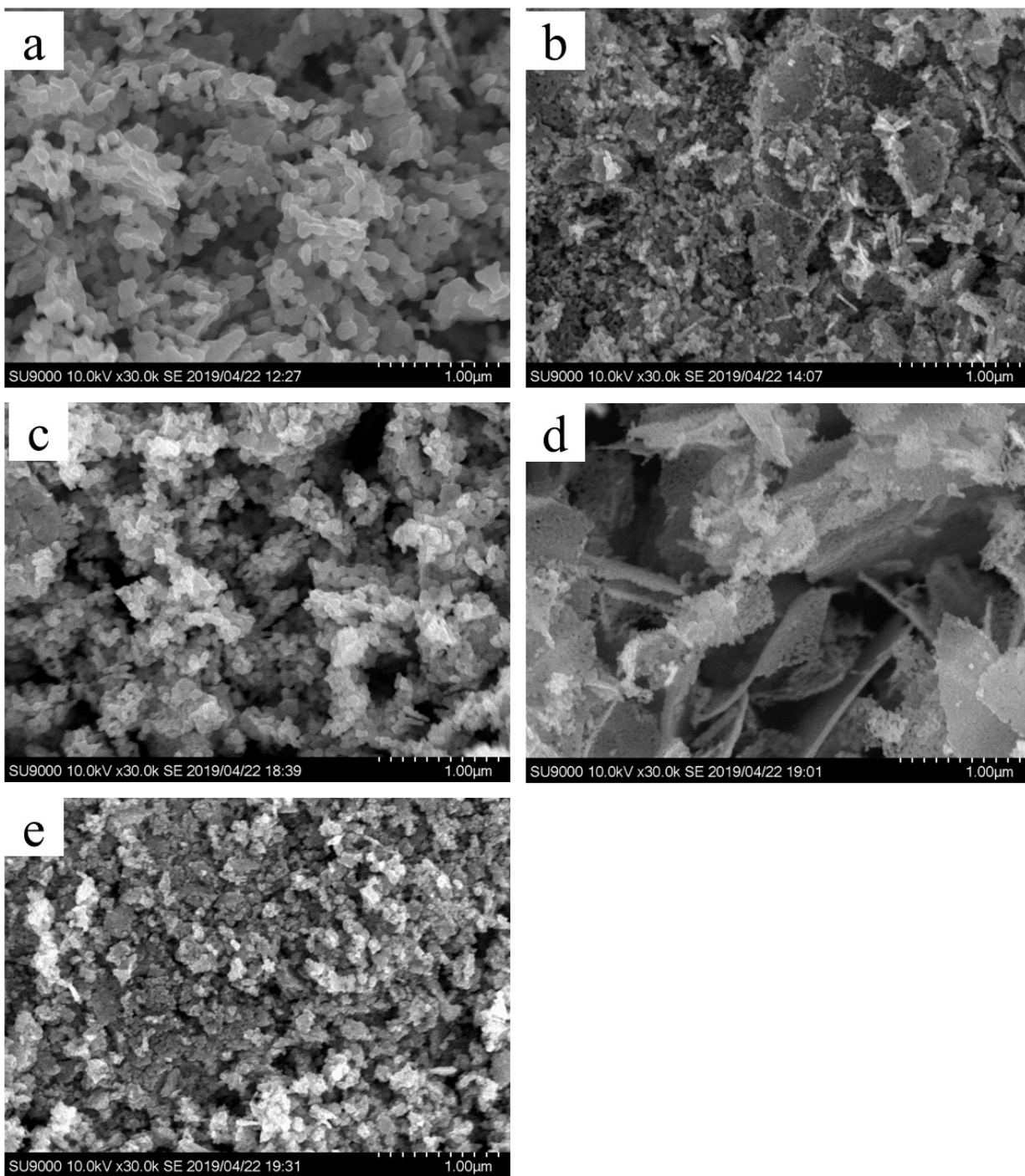
Fig. S5. SEM images of (a) $La_{0.8}Sr_{0.2}CoO_{3-\delta}$, (b) $La_{0.8}Sr_{0.2}Co_{0.8}Ni_{0.2}O_{3-\delta}$, (c) $La_{0.8}Sr_{0.2}Co_{0.8}Fe_{0.2}O_{3-\delta}$, (d) $La_{0.8}Sr_{0.2}Co_{0.8}Mn_{0.2}O_{3-\delta}$, and (e) $La_{0.8}Sr_{0.2}Co_{0.8}Cu_{0.2}O_{3-\delta}$.
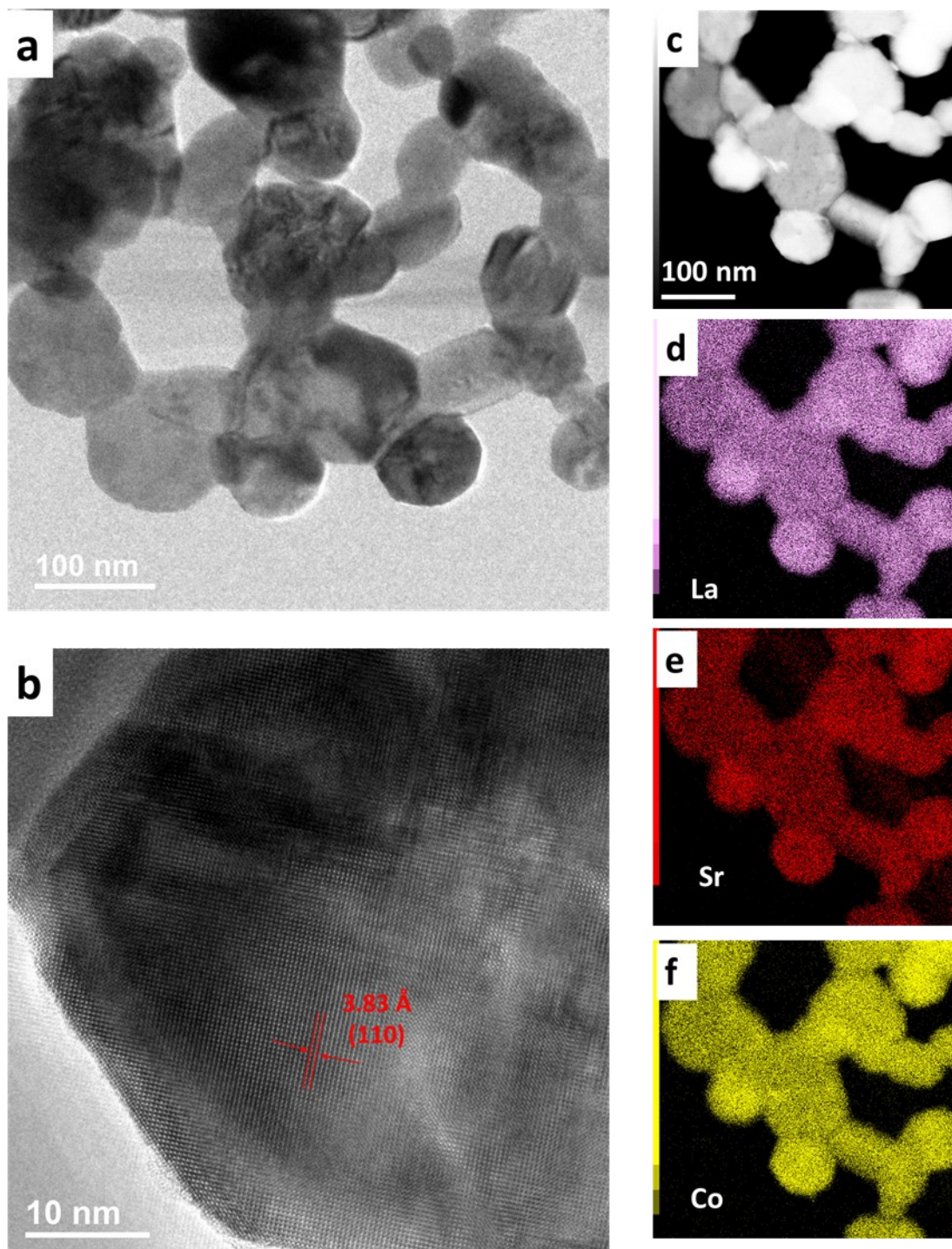
Fig. S6. (a) TEM image, (b) HRTEM image, (c) STEM image and (d–f) EDS elemental mappings (La, Sr and Co) of the $La_{0.8}Sr_{0.2}CoO_{3-\delta}$ perovskite oxide.
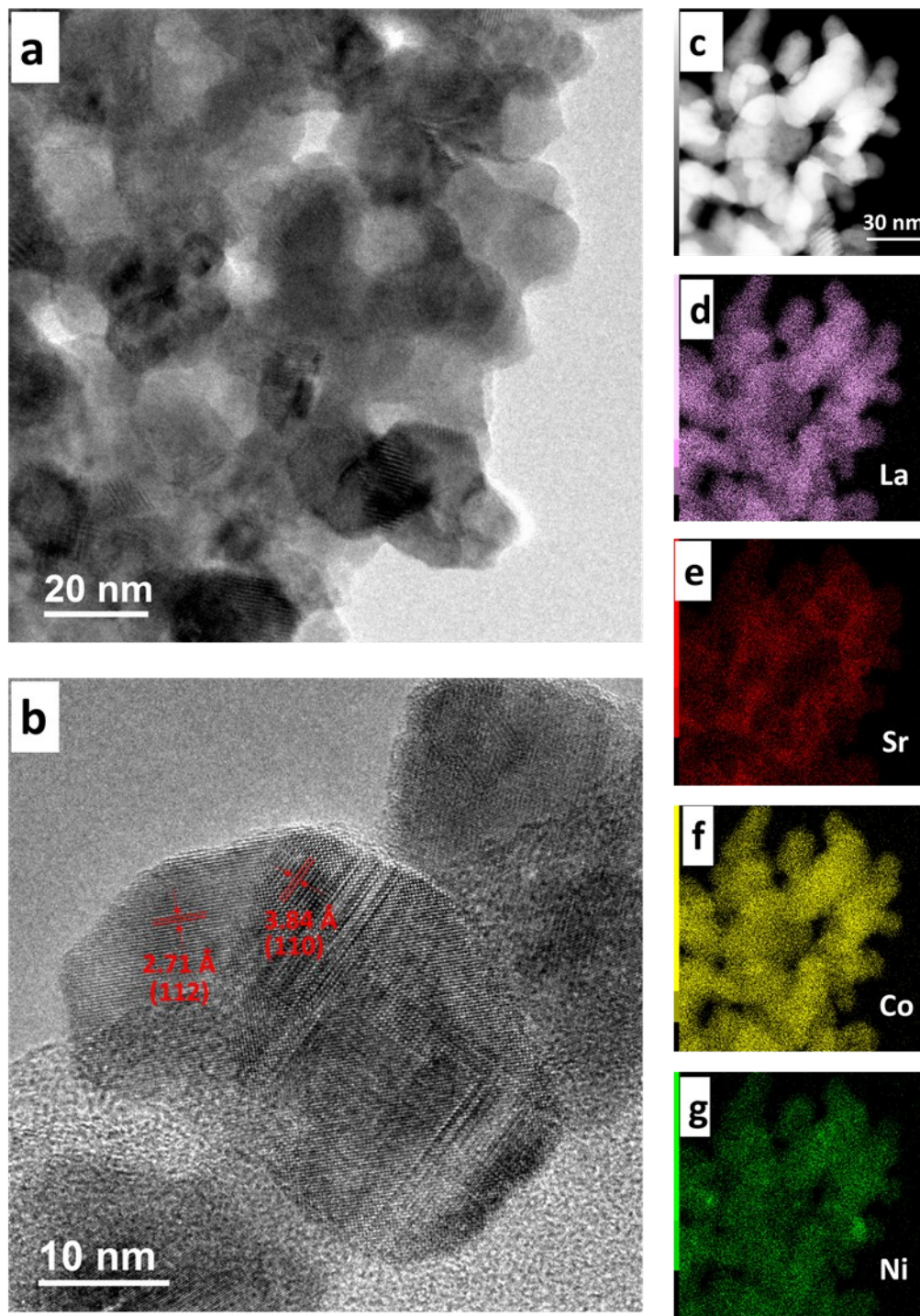
Fig. S7. (a) TEM image, (b) HRTEM image, (c) STEM image and (d–g) EDS elemental mappings (La, Sr, Cobalt-Co and Ni) of the $La_{0.8}Sr_{0.2}Co_{0.8}Ni_{0.2}O_{3-\delta}$ perovskite oxide.

Fig. S8. (a) STEM image, (b) HRTEM image, (c) STEM image and (d–g) EDS elemental mappings (La, Sr, Co, Mn) of the $La_{0.8}Sr_{0.2}Co_{0.8}Mn_{0.2}O_{3-\delta}$ perovskite oxide.
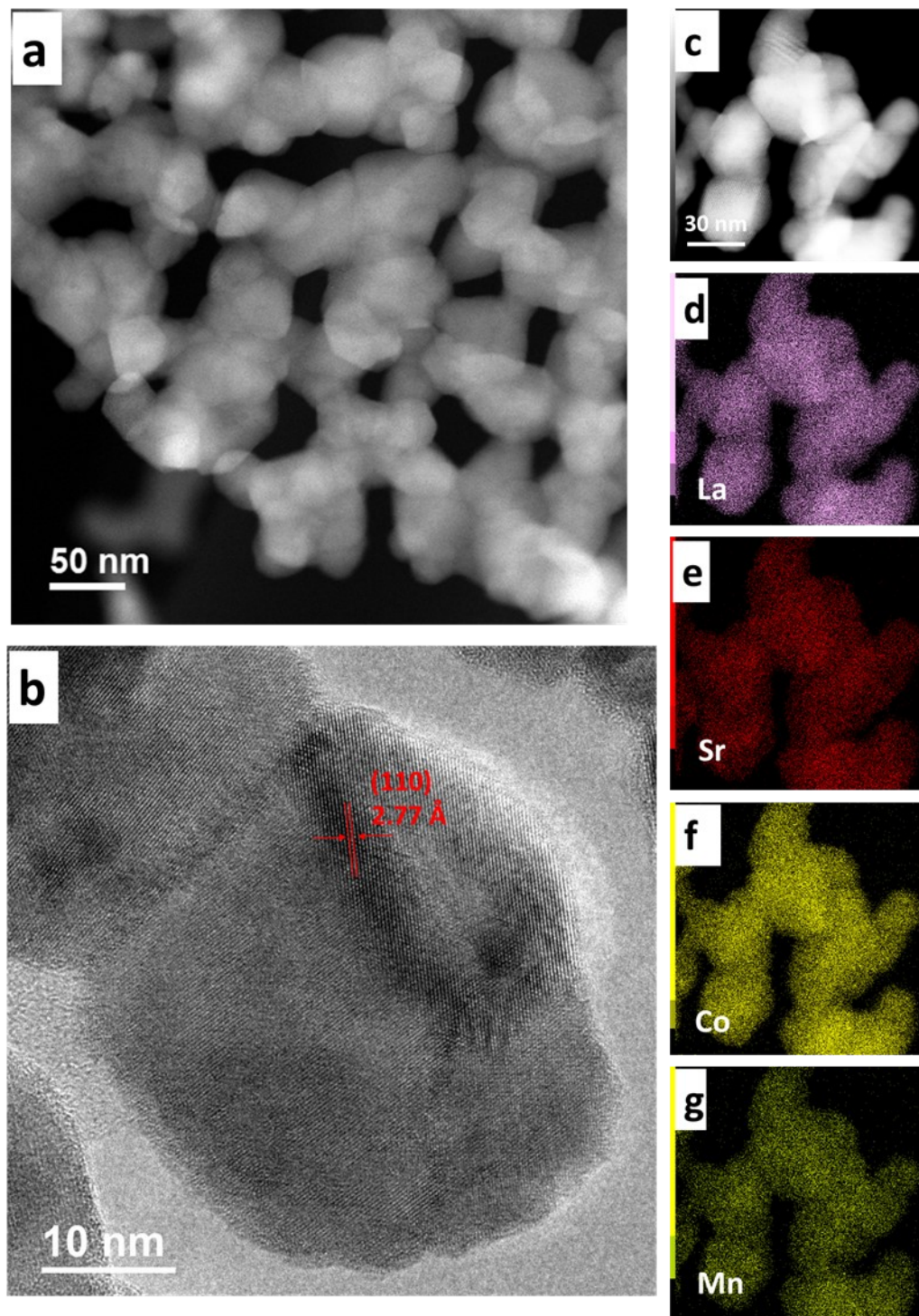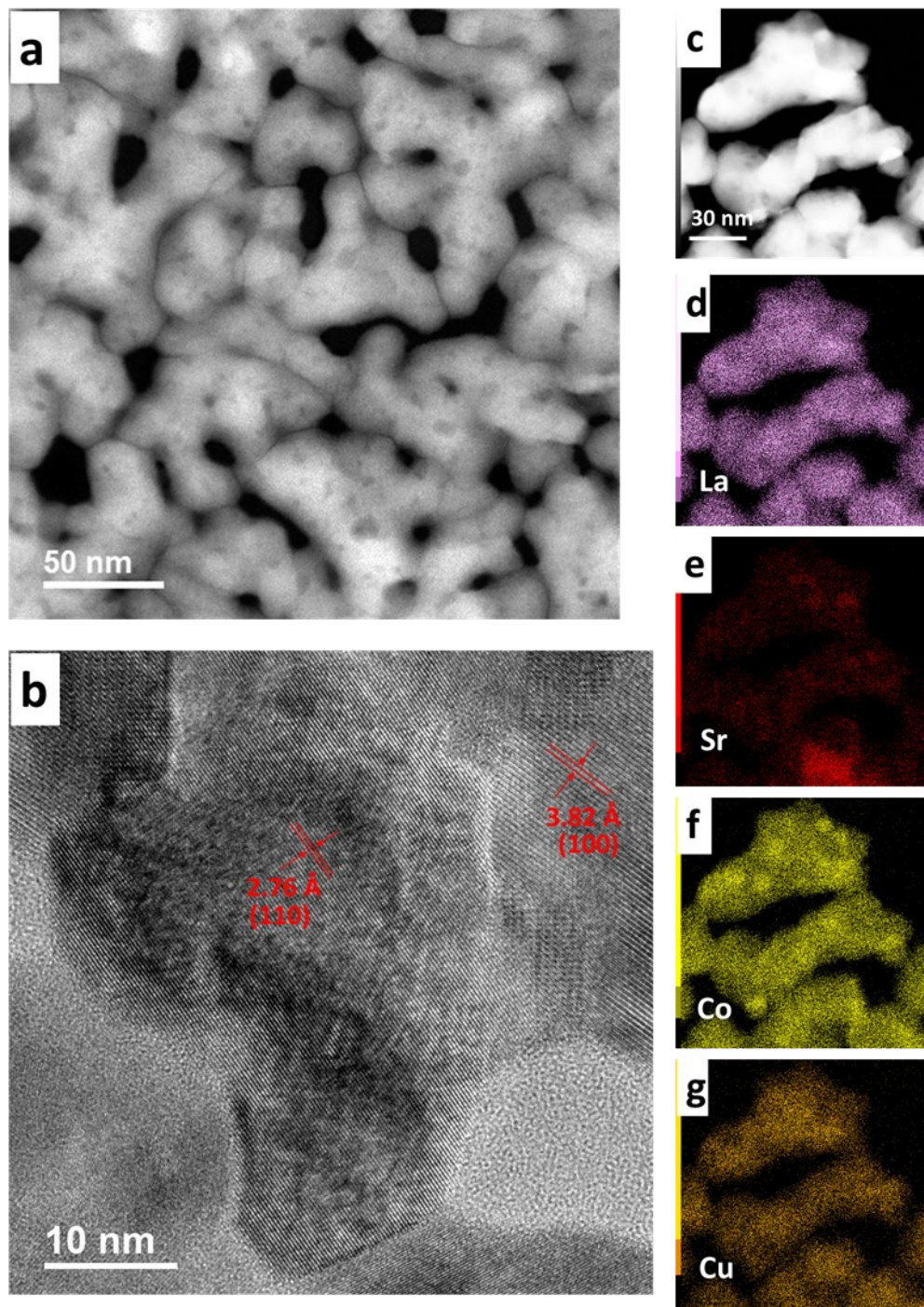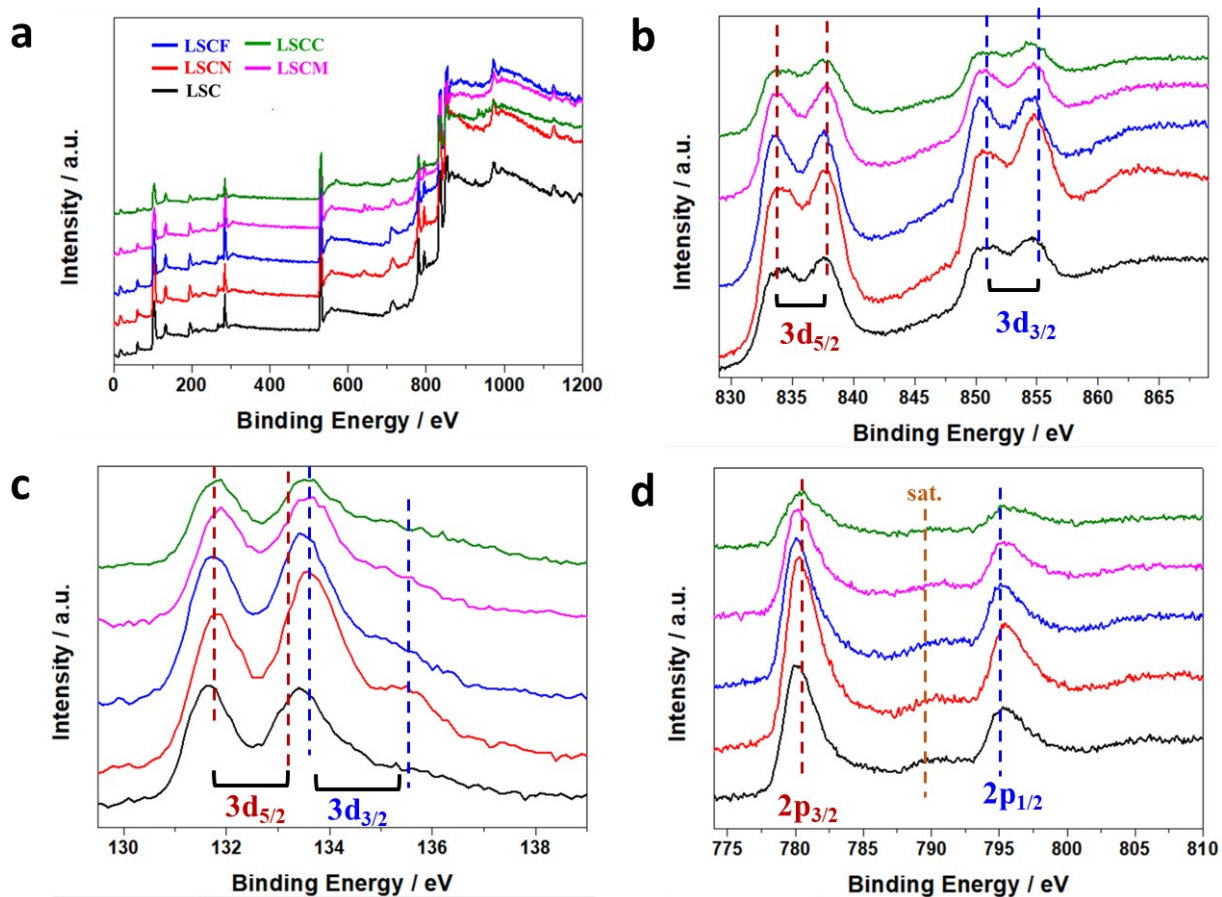
Fig. S9. (a) STEM image, (b) HRTEM image, (c) STEM image and (d–g) EDS elemental mappings (La, Sr, Co and Cu) of the $La_{0.8}Sr_{0.2}Co_{0.8}Cu_{0.2}O_{3-\delta}$ perovskite oxide.

Fig. S10. (a) XPS spectra of LSC, LSCN, LSCF, LSCM and LSCC perovskite oxides: (a) Survey, (b) La 3d, (c) Sr 3d and (d) Co 2p.
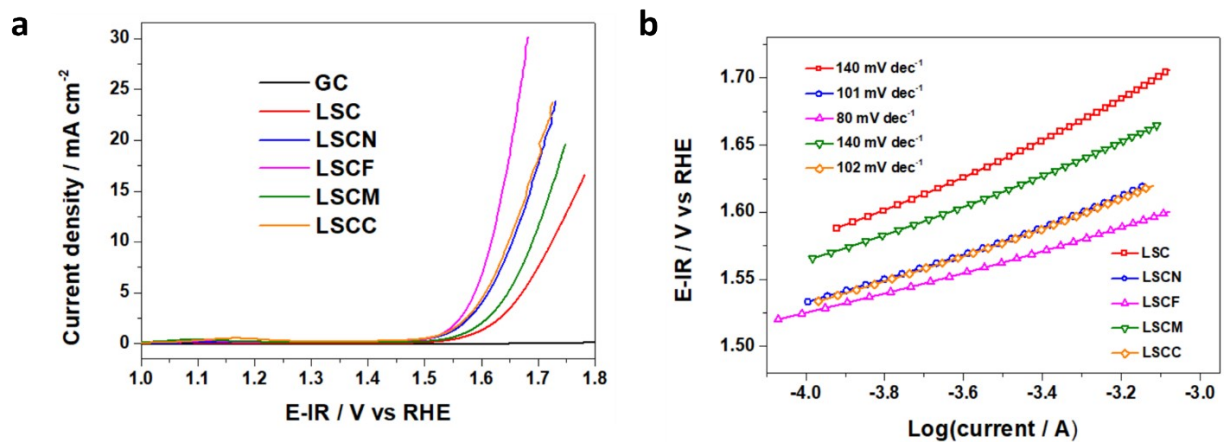
Fig. S11. (a) LSV OER curves of provided perovskite catalysts in 0.1M KOH at 1600 rpm, and (b) Tafel plots of OER for various catalysts in 0.1M KOH at 1600 rpm.
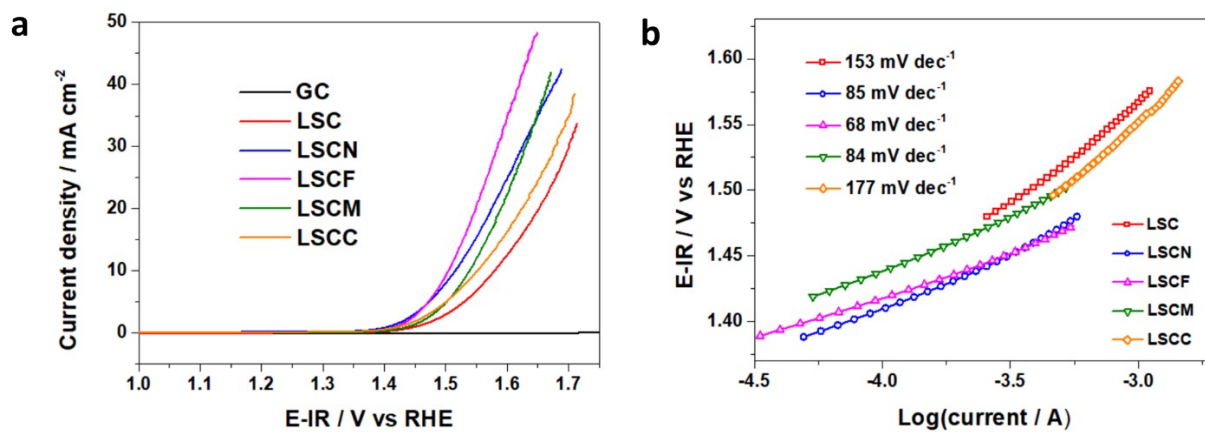
Fig. S12. (a) LSV OER curves of provided perovskite catalysts in 1M KOH at 1600 rpm, and (b) Tafel plots of OER for various catalysts in 1M KOH at 1600 rpm.
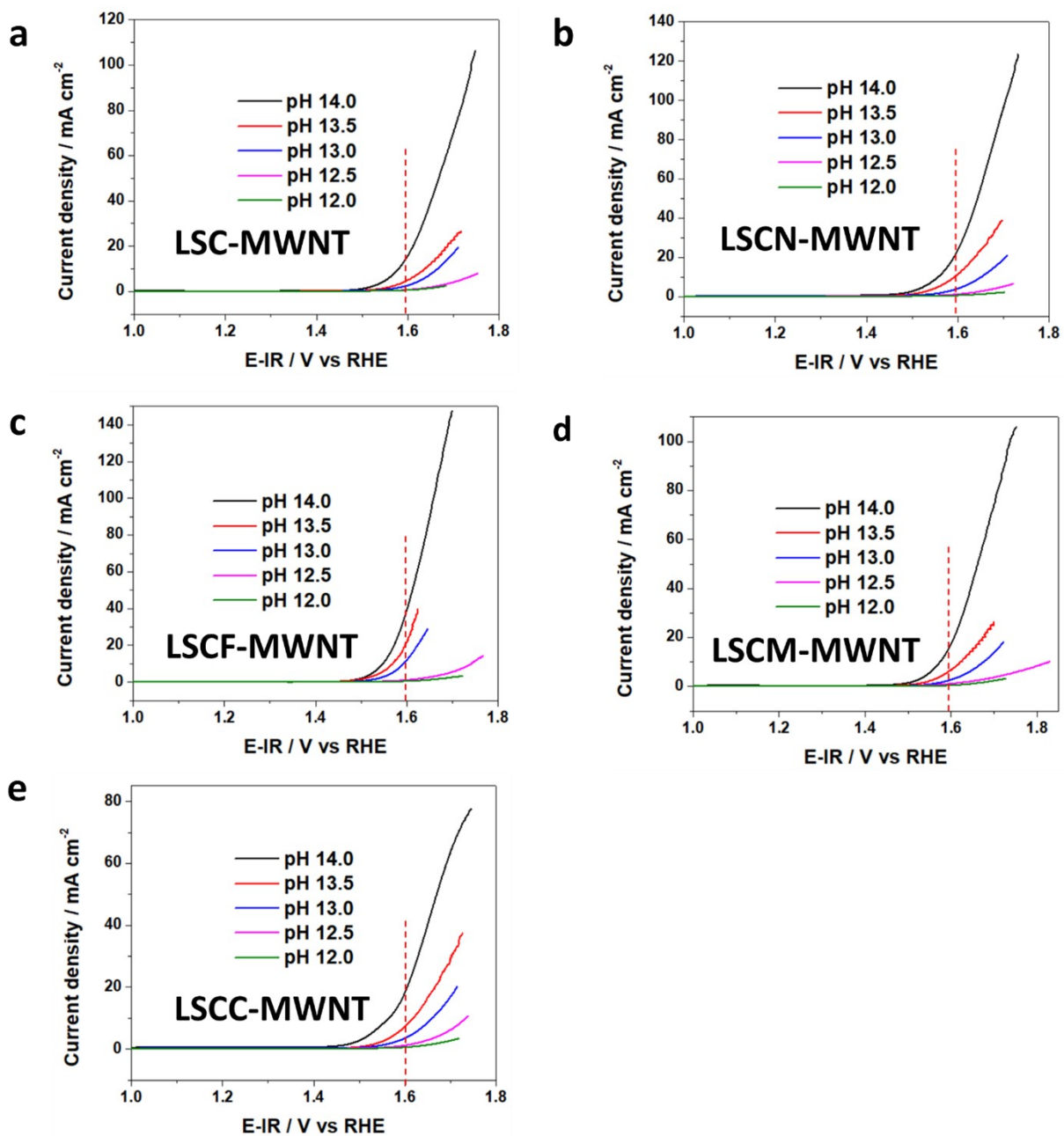
Fig. S13. OER activities of (a) LSC-MWNT, (b) LSCN-MWNT, (c) LSCF-MWNT, (d) LSCM-MWNT and (e) LSCC-MWNT in specified pHs at 1600 rpm.
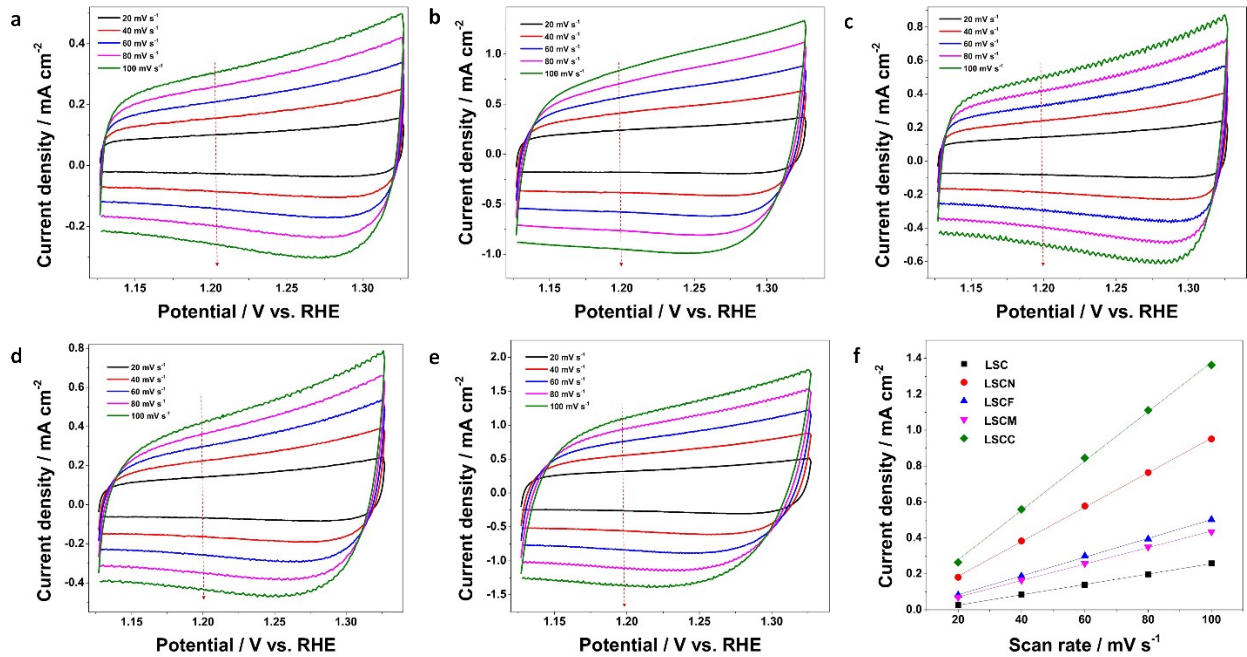
Fig. S14. CV curves of (a) LSC, (b) LSCN, (c) LSCF, (d) LSCM and (e) LSCC in the potential range of 1.1~1.35 V vs RHE at different scan rates from 20 to 100 mVs^{-1}; (f) C$_{dl}$ of LSC, LSCN, LSCF, LSCM and LSCC from the correlation between the current density and different scan rates from 20 to 100 mVs^{-1} based on CVs.
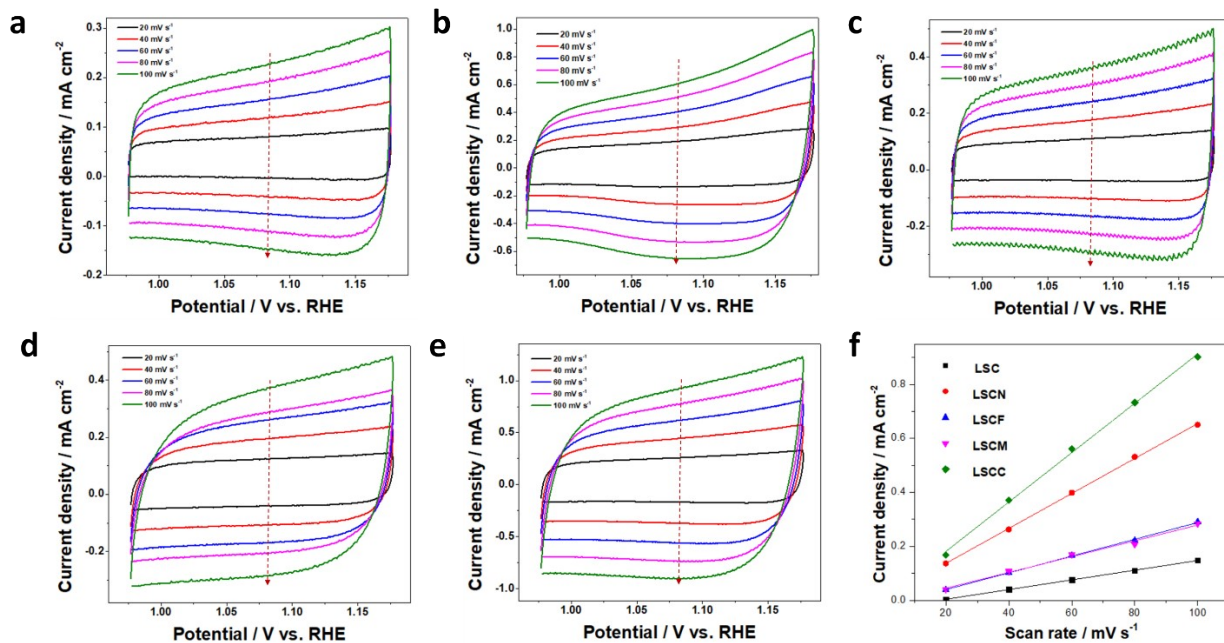
Fig. S15. CV curves of (a) LSC, (b) LSCN, (c) LSCF, (d) LSCM and (e) LSCC in the potential range of 1.00~1.15 V vs RHE at different scan rates from 20 to 100 mVs^{-1}; (f) C_{dl} of LSC, LSCN, LSCF, LSCM and LSCC from the correlation between the current density and different scan rates from 20 to 100 mVs^{-1} based on CVs.
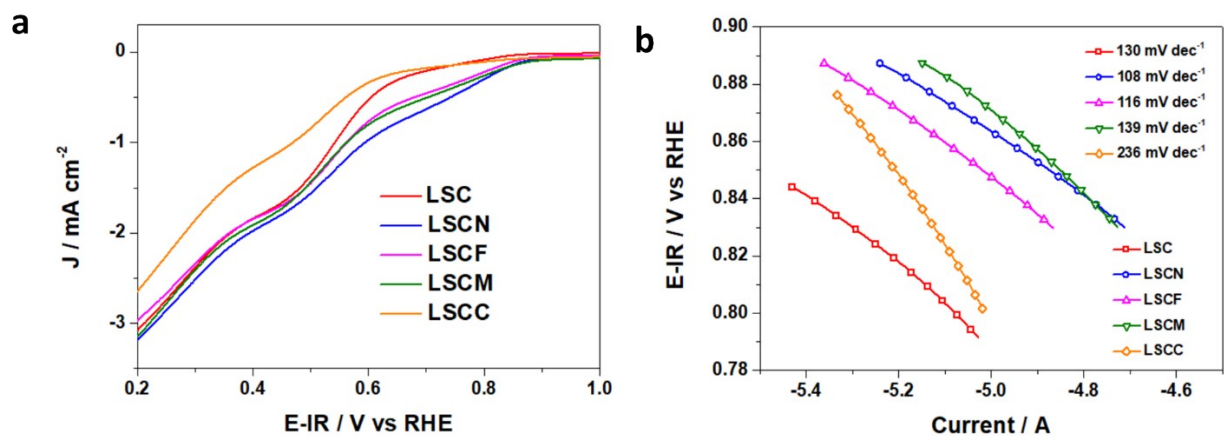
Fig. S16. LSV ORR curves of provided perovskite catalysts in 0.1 M KOH at 1600 rpm, while bubbling O_2; (b) Tafel plots of ORR for various catalysts in 0.1 M KOH at 1600 rpm.
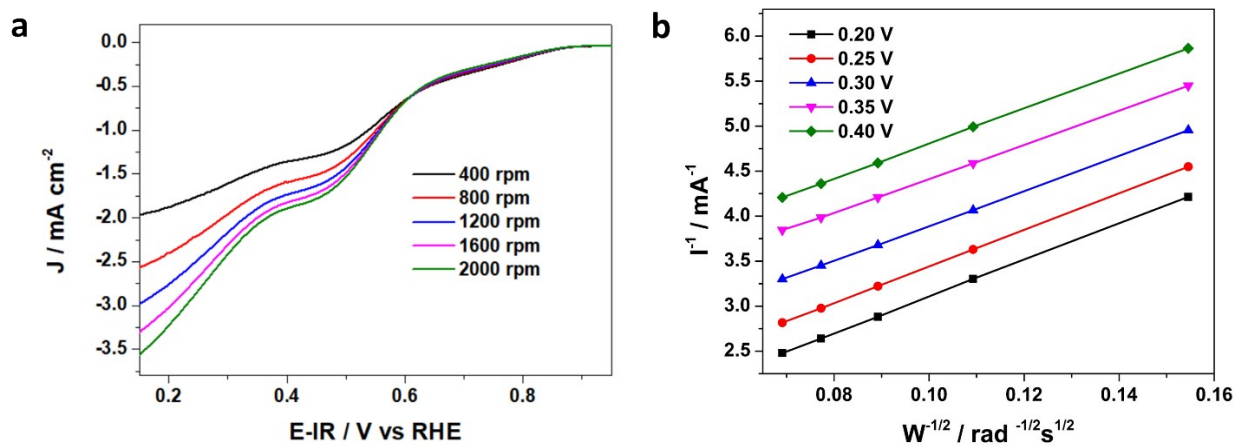
Fig. S17. (a) LSV ORR curves of LSCF in 0.1M KOH at 400, 800, 1200, 1600 and 2000 rpm and (b) the corresponding K-L plots.

The method of calculating the electron-transfer-numbers of LSCF during ORR

$1/K = 0.62 * n * F * A * v^{-1/6} * C_0 (D_0)^{2/3}$

Faraday constant (F) = 96485 A.s/mol

O_2 concentration (C_0) = 1.2 x 10^{-3} = 0.0012

Area of the electrode (A) = 0.1256 cm^2

Diffusion Coefficient of O_2 (D_0) = 1.9 x 10^{-5} cm^2 s^{-1}, $(D_0)^{2/3}$ = 7.12010 * 10^{-4}

Kinematic viscosity (v) = 0.01 cm^2/s, $v^{-1/6}$ = 2.15443

1/K is the slope value of the plotted K-L plots in Fig. S17a.

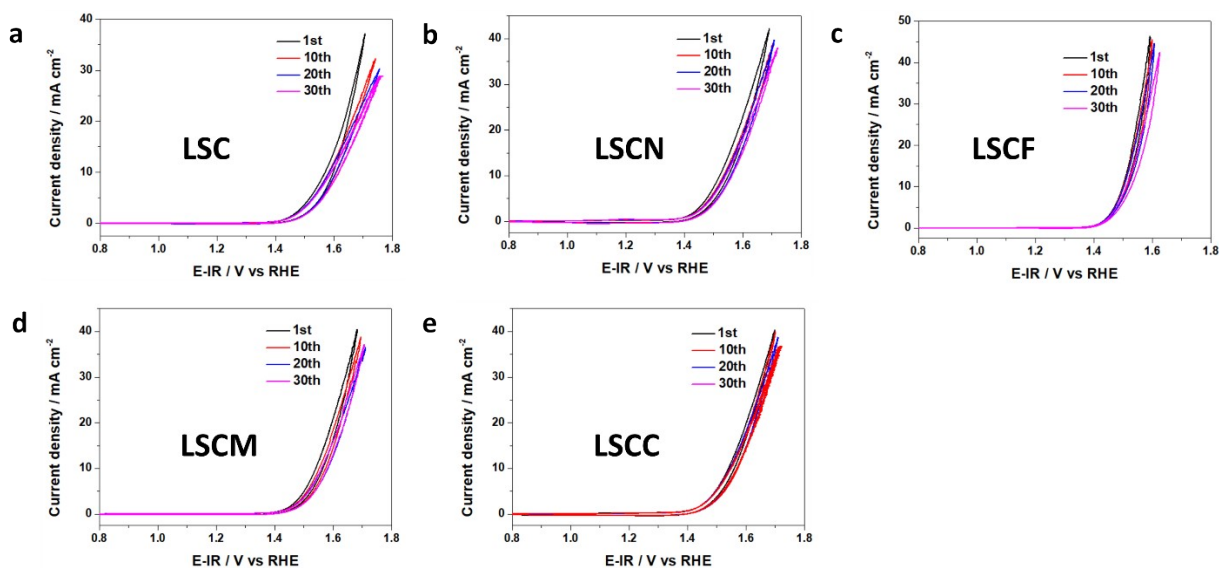# Cycles durability of the obtained perovskite oxides

Catalyst leaching or capacitive currents may substantially increase electrochemical currents. Therefore, anodic/cathodic single LSV scan is insufficient to confirm catalytic properties of the material. Fig. S14 and Fig. S15 suggest perceptible capacitance of the sample series and Fig.S16 (ORR measurements of perovskite oxides without MWNTs) suggests high leaching rates of our catalysts. Therefore, we measured the CV cycles of the obtained perovskite oxides, and the obtained results are shown in Fig. S18. The CV curves of the first cycle are similar with the LSV plots. Besides, CV cycles of LSC show some attenuation during 30 cycles, while the attenuation is not obvious for LSCN, LSCF, LSCM and LSCC catalysts, which indicated that the B-site doping is beneficial for the electrochemical stability of perovskite oxides.

Fig. S18. CV cycles durability of (a) LSC, (b) LSCN, (c) LSCF, (d) LSCM and (e) LSCC in 1M KOH electrolyte.

Table S1. The comparison of OER activities between the perovskite catalysts in this study and the reported state-of-the-art perovskite oxides.

Samples	electrolyte		$E_{OER}@10mA\ cm^{-2}$		Reference
LSC-MWNT	0.1 M KOH	1 M KOH	1.66	1.60	*This study*
LSCN-MWNT			1.65	1.58	
LSCF-MWNT			1.59	1.56	
LSCM-MWNT			1.67	1.59	
LSCC-MWNT			1.66	1.58	
$LaCoO_3$	0.1 M KOH	-	~1.64	-	*Chem. Mater. 2015, 27, 7662−7672*
$La_{0.8}Sr_{0.2}CoO_3$			~1.59	-	
$La_{0.6}Sr_{0.4}CoO_3$			~1.61	-	
$La_{0.4}Sr_{0.6}CoO_3$			~1.62	-	
$La_{0.2}Sr_{0.8}CoO_3$			~1.62	-	
$LaCoO_3$	0.1 M KOH	-	> 1.68	-	*ACS Sustainable Chem. Eng. 2017, 5, 10910−10917*
Porous $LaCoO_3$			> 1.64	-	
Hollow nanospheres $LaCoO_3$			> 1.63	-	
La_xMnO_3	0.1 M KOH		> 1.70	-	*Electrochimica Acta 333 (2020) 135566*
$Ba_{0.5}Sr_{0.5}Co_{0.8}Fe_{0.2}O_{3-\delta}$	0.1 M KOH	-	~1.61	-	*J. Phys. Chem. C 2013, 117, 8628−8635*
$SrCo_{0.8}Fe_{0.2}O_{3-\delta}$			> 1.64	-	
$LaCoO_3$			> 1.65	-	
$Ba_{0.5}Sr_{0.5}Co_{0.8}Fe_{0.2}O_{3-\delta}$	0.1 M KOH	-	~1.59	-	*J. Phys. Chem. Lett. 2012, 3, 3264−3270*
$LaCoO_3$			> 1.68	-	
$La_{0.5}Sr_{0.5}Ni_xFe_{1-x}O_{3-\delta}$	0.1 M KOH	-	~1.59-1.72		*Electrochimica Acta 246 (2017) 997–1003*

Material					Reference
LaMn$_x$Co$_{1-x}$O$_3$	0.1 M KOH		~1.65-1.68		*ACS Appl. Mater. Interfaces 2020, 12, 24717−24725*
LaCoO$_3$			1.71		
La$_{1.5}$Sr$_{0.5}$NiMn$_{0.5}$Ru$_{0.5}$O$_6$	0.1 M KOH		1.66		*ACS Appl. Mater. Interfaces 2019, 11, 21454−21464*
Ba$_2$CoMo$_{0.5}$Nb$_{0.5}$O$_{6-\delta}$	0.1 M KOH		1.66		*ACS Appl. Mater. Interfaces 2018, 10, 16939−16942*
BaCoO$_{3-\delta}$			1.75		
La$_{1-x}$Sr$_x$FeO$_{3-\delta}$	0.1 M KOH		1.6-1.75		*ACS Appl. Mater. Interfaces 2018, 10, 11715−11721*
BaCo$_{0.9-x}$Fe$_x$Sn$_{0.1}$O$_{3-\delta}$	0.1 M KOH		~1.66-1.7		*Adv. Sci. 2016, 3, 1500187*
Hollow Multishelled LaCo$_{1-x}$Ni$_x$O$_{3-\delta}$	0.1 M KOH		~1.56-1.6		*Angew. Chem. Int. Ed. 2020, 59, 19691–19695*
CQDs@BSCF-NFs	0.1 M KOH		~1.6		*Applied Catalysis B: Environmental 257 (2019) 117919*
BSCF-NFs			~1.64		
Ba$_{0.5}$Sr$_{0.5}$Co$_{0.8}$Fe$_{0.2}$O$_{3-\delta}$ (BSCF)			~1.67		
La$_{0.8}$Sr$_{0.2}$CoO$_3$	0.1 M KOH		~1.66		*Journal of The Electrochemical Society, 161 (6) F694-F697 (2014)*
La$_{0.6}$Sr$_{0.4}$Co$_x$Fe$_{1-x}$O$_{3-\delta}$	0.1 M KOH		~1.55-1.64		*Progress in Natural Science: Materials International 28 (2018) 399–407*
La$_{0.5}$Sr$_{0.5}$Co$_{0.8}$Fe$_{0.2}$O$_3$-PR/NRGO	0.1 M KOH		~1.7		*Nano Energy(2014) 10, 192–200*
P-doped LaFeO$_{3-\delta}$	0.1 M KOH		~1.67-1.75		*Nano Energy 47 (2018) 199–209*
LaCr$_{0.5}$Fe$_{0.5}$O$_3$	0.1 M KOH		1.61		*Scientific Reports Vol. 10, Iss. 1, (2020). DOI:10.1038/s41598-020-70283-9*
La$_{0.4}$Sr$_{0.6}$Co$_{0.7}$Fe$_{0.2}$Nb$_{0.1}$O$_{3-\delta}$	0.1 M KOH		1.6-1.65		*International Journal of Hydrogen Energy 45 (2 0 2 0) 3 0 5 8 3-3 0 5 9 1*
La$_{1-x}$Sr$_x$Co$_{1-y}$Fe$_y$O$_{3-\delta}$		1 M KOH		~1.66	*ACS Appl. Energy Mater. 2018, 1, 3342−3350*
La$_{0.6}$Sr$_{0.4}$CoO$_{3-\delta}$	0.1 M KOH		~1.72-1.76		*Energy Fuels 2020, 34, 16838−16846*
La$_{0.6}$Sr$_{0.4}$Co$_{0.8}$Fe$_{0.2}$O$_3$	0.1 M KOH		~1.61-1.67		*Applied Surface Science 529 (2020) 147165*
La$_{0.5}$Sr$_{0.5}$MnO$_3$-80-Co	0.1 M KOH		~1.67		*Nano Energy 71 (2020) 104564*
Sm$_{0.5}$Sr$_{0.5}$CoO$_{3-\delta}$ hollow nanofibers	0.1 M KOH		~1.61		*Small 2018, 14, 1802767*
La$_{0.4}$Sr$_{0.6}$Ni$_{0.5}$Fe$_{0.5}$O$_3$		1 M KOH		~1.56	*Front. Chem. 7:224. doi: 10.3389/fchem.2019.00224*

Note: The listed catalysts are tested with different carbon materials, which are not specified in the sample names.

Table S2. The Cartesian coordinates of $La_{0.80}Sr_{0.20}Ni_{0.20}Co_{0.80}O_3$ used for the simulated XRD pattern.

Elements	X co-ordinate	Y Co-ordinate	Z co-ordinate
La	0.5	0.53	0.25
O1	2.037	1.482	1.25
O2	2.0	1.5	0.5
Co	2.0	1.5	0.5
Sr	1.5	0.5	0.5
Ni	2.0	1.5	0.5